

Deepening the understanding of cosmic-ray diffusion

P. Reichherzer^{1,2}, J. Becker Tjus^{1,2}, E.G. Zweibel^{3,4}, L. Merten^{1,2,5}, and M.J. Pueschel⁵

¹ *Theoretical Physics IV: Plasma-Astroparticle Physics,*

Faculty for Physics & Astronomy, Ruhr-Universität Bochum, 44780 Bochum, Germany

² *Ruhr Astroparticle And Plasma Physics Center (RAPP Center)*

³ *Department of Astronomy, University of Wisconsin-Madison, Madison, WI 53706, U.S.A.*

⁴ *Department of Physics, University of Wisconsin-Madison, Madison, WI 53706, U.S.A.*

⁵ *Institute for Astro- & Particle Physics,*

University of Innsbruck, 6020 Innsbruck, Austria

⁶ *Institute for Fusion Studies, University of Texas at Austin, Austin, TX 78712, U.S.A.*

Abstract

For the first time, we characterize the rigidity regimes of the diffusion coefficient κ for arbitrary rigidities and guide fields, which we derive as a function of physical and numerical parameters. We show that at turbulence levels above 5% of the total magnetic field, the approximation of an energy dependence $\kappa \propto E^{1/3}$ as predicted for a Kolmogorov spectrum within Quasi-Linear Theory does not hold. Consequently, a proper description of cosmic-ray propagation can only be achieved by using a turbulence-level dependent diffusion coefficient and can contribute to solving the Galactic cosmic-ray gradient problem.

INTRODUCTION

Cosmic-ray diffusion is believed to be the dominant process for the transport of cosmic rays in many astrophysical environments [1–3]. In particular, the leaky box model of the Milky Way predicts that the cosmic-ray energy spectrum observed at Earth is steepened by diffusion: the spectrum is composed of the ratio of the source spectrum $Q(E) \propto E^{-\alpha}$ and the diffusion coefficient $\kappa(E) \propto E^\gamma$, i.e., $N(E) \propto E^{-\alpha-\gamma}$ [4]. These arguments are based on Quasi-Linear Theory (QLT), in which cosmic-ray propagation in an isotropic wave-vector spectrum $G(k) \propto E^{-5/3}$ leads to a parallel diffusion coefficient $\kappa \propto E^{1/3}$ [5, 6]. Numerical simulations of particle transport in a combination of turbulent field b and homogeneous field B , were in accordance with this spectral index up to high $b/B \sim 1$ [8, 9, 45]. These simulations are typically performed in a controlled plasma environment, i.e. a 3-dimensional cartesian grid structure with a spacing s and a number of grid points N_{grid} is used to inject relativistic particles from a point source in a homogeneous ($\vec{B} = B\vec{e}_z$) plus turbulent (\vec{b}) magnetic field in order to calculate the diffusion coefficient. Radiative losses are not considered. Recent studies have pointed out that these results need to be interpreted carefully, as the energy range in which the simulations are fully diffusive is strongly limited [10–13]. Here, for the first time, we present the classification of the diffusion coefficient in five different regimes. With this characterization of the validity range of the diffusive regime, we perform simulations that quantitatively investigate the spectral behavior of the diffusion coefficient with energy. We show the importance of the turbulence level with respect to the spectral behavior and argue that these findings are in accordance with the cosmic-ray gradient that is observed in the Galaxy.

THE FIVE REGIMES OF THE DIFFUSION COEFFICIENT

Based on our findings in the simulation (see supplement for examples) and from theoretical arguments, we identify five different propagation regimes. It is the *resonant scattering regime* (RSR) that corresponds to QLT, with a predicted energy dependence $\kappa \propto E^{1/3}$ for a Kolmogorov-type wavevector spectrum $G(k) \propto k^{-5/3}$. We find that the energy range for this regime is limited by the lower and upper turbulence scales of the system l_{min} and l_{max} , respectively. The reason is that particles with gyroradius r_g interact with waves according

to the gyro-resonance criterion $\omega - k_{\parallel}v_{\parallel} = n\Omega$, where k_{\parallel} and v_{\parallel} are the wavenumber of the fluctuation and the velocity of the particle parallel to the mean magnetic field. The relativistic gyrofrequency of the charged particle is denoted by Ω and n is a positive or negative integer. The frequency ω of the fluctuation is expected to be $\omega \sim kv_A$ for MHD fluctuations and can consequently be neglected for relativistic particles $v \sim c \gg v_A$. With this reasoning, the gyro-resonance criterion is $k = 2\pi/l = (\mu r_g)^{-1}$. Thus, for arbitrary pitch angles $0 \leq |\mu| = |\cos \theta| \leq 1$, not all particles find waves to resonate with when the limits of the wavevector spectrum are reached.

In order to quantify this effect and thereby the resonant-scattering transition, i.e. from partially to fully diffusive transport, we introduce the reduced rigidity $\rho \equiv r_g/l_c$. We use this definition as $\kappa_{\parallel} = cl_c(r_g/l_c)^{\gamma}(B/b)^2$ and thus, κ_{\parallel} scales with ρ . Here, the correlation length $l_c = (c/b^2) \int_0^{\infty} dt \langle b(x(t))b(x(0)) \rangle$ of the turbulent magnetic field b and the gyroradius $r_g = R/B$ are introduced, where $R = p/q$ (momentum over charge) is the rigidity. The behavior of $\kappa(\rho)$ can be interpreted in terms of an energy dependence and provides a validity for a relatively large parameter space as demonstrated in the supplement.

In the following, we quantify the regimes in order of increasing ρ according to the expected transition with respect to resonant scattering within a range of length scales $l_{\min} \leq l \leq l_{\max}$ and discuss their origin.

1. *Non-Resonant Scattering Regime (NRSR)*: For $\rho \lesssim l_{\min}/(2\pi l_c)$, particles cannot scatter resonantly, as $|\mu| = \frac{l}{2\pi r_g}$ cannot be fulfilled. The smaller the reduced rigidity, the larger the effect, while the parallel diffusion coefficient is expected to increase toward low ρ . Because of the small gyroradius in combination with a large parallel diffusion coefficient for small reduced rigidities, particles follow field lines for a long time.
2. *Mirror Regime (MR)*: At values $l_{\min}/(2\pi l_c) \lesssim \rho \lesssim l_{\min}/(\pi l_c (b/B))$, particles scatter resonantly given appropriate pitch angles. As scattering is prohibited for parts of the pitch angle spectrum, mirroring occurs instead [11, 14–16]. Two effects oppositely affect the diffusion coefficient with reduced rigidity: the missing pitch angles enhance diffusion, while mirroring reduces parallel diffusion. Thus, the diffusion coefficient decreases somewhat above the boundary $\rho \sim r_g/l_{\min}$ but then increases toward the upper end of the MR, because the range of pitch angles that can scatter resonantly is widening until the resonant scattering regime is reached.

3. *Resonant Scattering Regime (RSR)*: For $l_{\min}/(\pi l_c (b/B)) \lesssim \rho \lesssim l_{\max}/(2\pi l_c)$, particles can scatter resonantly for almost all μ - they still cannot scatter at $\mu = 0$, but via pitch angle fluctuations $\delta\mu$, they are able to scatter over that gap from $-\mu_{\min}$ to $+\mu_{\min}$ and vice versa. This phenomenon explains the lower boundary condition as follows: A gyroresonant wave produces a change in pitch angle $\delta\mu$ of order $\delta\mu \approx b/B$ when scattered once [17]. Presuming that successive scatterings are uncorrelated and can be treated as a random walk, and that the cosmic rays encounter one wave per gyroorbit, then the corresponding diffusion coefficient in pitch angle space is $D_{\mu\mu} = (\Delta\mu)^2/\Delta t \sim \omega_c (b/B)^2$, with $\Delta\mu$ the scattering angle after many scatterings and ω_c as the gyro frequency. The corresponding spatial diffusion coefficient is $v^2/D_{\mu\mu}$. Particles can scatter over the gap at $\mu = 0$, i.e. over the distance of $\Delta\mu \sim b/B = \mu_{\min} - (-\mu_{\min}) = 2\mu_{\min}$. Thus, all possible pitch angles are available for scattering at $\rho > l_{\min}/(2\pi r_g \mu_{\min}) = l_{\min}/(\pi r_g b/B)$, setting the lower scale of this regime for a given ratio b/B . The upper boundary is defined by the condition that particles with gyroradii exceeding the injection scale cannot scatter resonantly.
4. *Transition Regime (TR)*: For $l_{\max}/(2\pi l_c) < \rho < 5 l_{\max}/(\pi l_c)$, the transition to the quasi-ballistic regimes occurs, as particles are again limited in their pitch-angle scattering, since l_{\max} is reached. The transition starts when the gyroradius approaches wavelengths of the size of the maximum scattering length $2\pi r_g \sim l_{\max}$. At larger values, the resonance condition again prevents scattering. Scattering likelihood decreases until the quasi-ballistic regime is reached at $\rho = 5 l_{\max}/(\pi l_c)$. The transition regime is expected to extend one order in the reduced rigidity [18].
5. *Quasi-Ballistic Regime (QBR)* For $\rho > 5 l_{\max}/(\pi l_c)$, scattering is only possible for $\mu \approx 0$, which is why we term this range quasi-ballistic. This criterion follows from $\mu = l_{\max}/(2\pi r_g) = 1$. Larger values for μ are not possible and thus define the point of transition out of the fully resonant scattering regime. With $l_{\max} = 5l_c$, this leads to $r_g = l_{\max}/(2\pi) = 5 \cdot l_c/(2\pi)$, which results in $\rho = r_g/l_c = 5/(2\pi)$. In QLT, the dependency of the diffusion coefficient becomes $\kappa \propto (B/b)^2 \rho^2 c l_c$, see, e.g., Ref. [19] and references therein.

The diffusion coefficient for a broad range of ρ is displayed in Fig. 1a. Figure 1b shows the fraction of pitch angles that are available for scattering, indicating that the RSR is the

only range in which all angles are accessible. The two different contributions to the light blue area are derived in Fig. 1c, which shows the pitch angle as a function of reduced rigidity together with the boundaries $(l_{\min}, l_{\max})/2\pi r_g$ and the gray boundary lines outside of which scattering is fully non-resonant. This effect is depicted in the two lower panels of Fig. 1 as the light blue area with vertical white lines into which particles are able to scatter on average. The blue area with dots indicates the parameter space which allows scattering according to the gyro-resonance criterion. With these considerations, we can now for the first time present simulation results for a fully defined RSR and compare to QLT.

For physically relevant conditions, the smallest scale is the dissipation level, i.e., $l_{\min} = l_{\text{diss}}$, while the largest scale is the turbulence injection scale $l_{\max} = l_{\text{inj}}$. In the context of global Galactic propagation, supernova remnants (SNRs) are believed to be responsible for injection, and thus the outer scale is expected to be on the order of $l_{\text{inj}}^{\text{Galaxy}} \approx 10 - 100$ pc [19]. Measurements of the wavevector spectrum set an upper limit to the injection scale of $l_{\text{diss}} \lesssim 10^9$ cm [20]. These values indicate that for Galactic propagation, the ratio of injection to dissipation scale required for simulation should be $l_{\max}/l_{\min} \gtrsim 3 \times 10^{11}$.

Current simulations usually employ grids with $N_{\text{grid}}^3 = 10^{10} - 10^{11}$ grid points, limited by available memory. The largest scale $l_{\text{high}} = N_{\text{grid}}s/2$ is related to the spacing s . Thus, for our simulations, the largest and smallest scales are given either by simulation requirements or by physical conditions: $l_{\min} = \max(l_{\text{diss}}, 2s)$ and $l_{\max} = \min(l_{\text{inj}}, l_{\text{high}})$. Only one of the two can be set independently. As the injection scale is typically linked to turbulence injection by SNRs, this, together with the computational limitations on N_{grid} , typically determines a lower scale for the simulations above the physical dissipation scale. Thus, for a part of the spectrum, wavelengths for the particle-wave interactions are missing that would be present in the physical situation. Thus, in Fig. 1, particularly the transitions that include l_{\min} usually cannot be interpreted in a physical way, but stem from this numerical effect.

SIMULATIONS OF THE DIFFUSIVE REGIME

Our simulations are based on the well-established Taylor-Green-Kubo (TGK) formalism [21], see, e.g., Ref. [8–10, 12, 13, 18, 22, 45]. Building on previous work in the area that focused on specific parameter points and resolutions, we conduct a systematic and careful analysis that reveals key conditions on numerical simulation requirements. This method

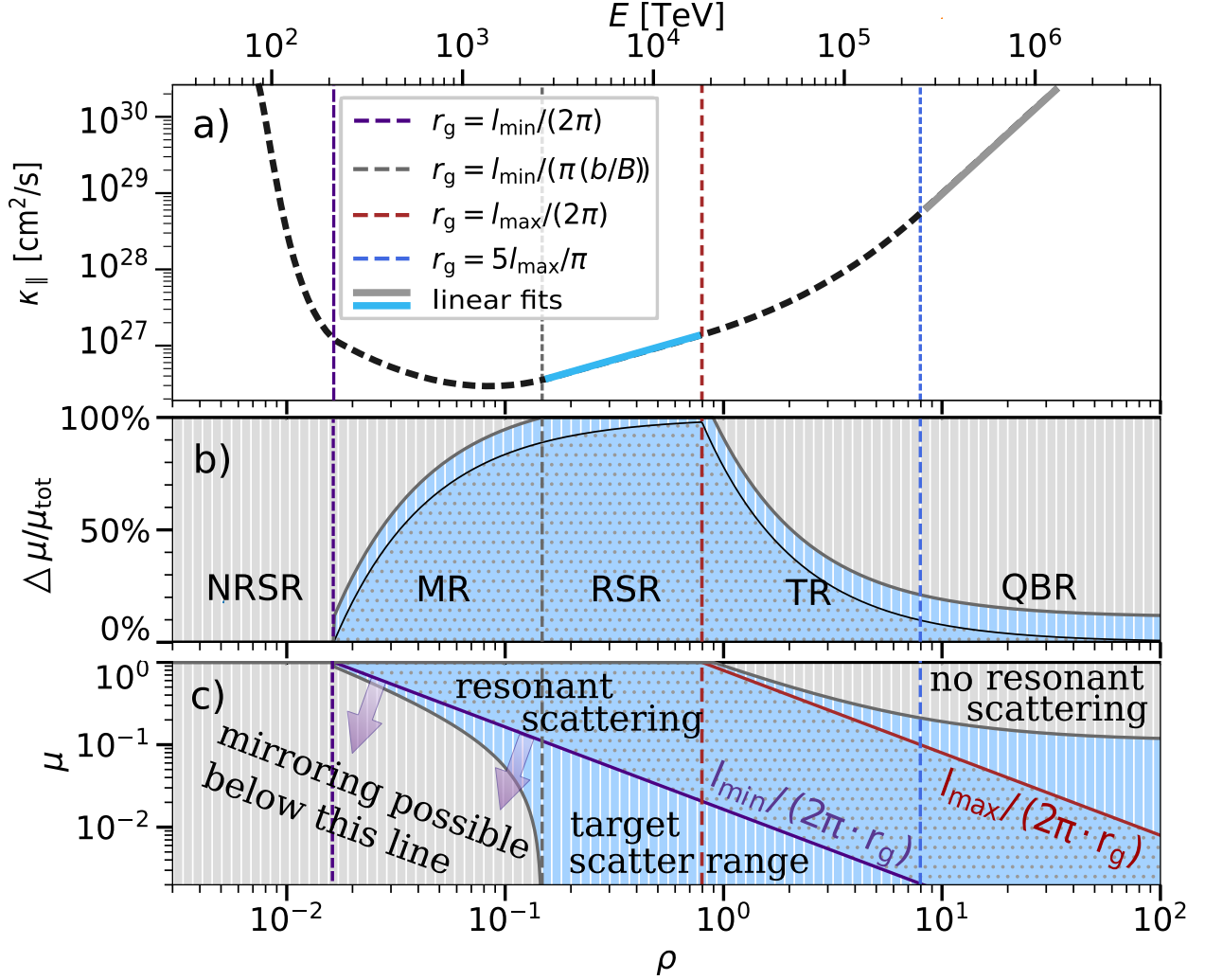


FIG. 1. The diffusion coefficient as a function of reduced rigidity for the five regimes a) and the corresponding fraction of pitch angles available for scattering (b), as well as the pitch angle (c) with the indicated ranges of possible scattering and mirroring. In panels b) and c), in the gray, horizontally-striped areas, no (c) or not all (b) pitch angles are available for scattering. In b) and c), the blue, dotted area represents those pitch angles that are allowed by the gyro-resonance condition. The blue, striped area represents the scattering that occurs due to fluctuations $\delta\mu \sim (b/B)$.

uses that the fundamental solution for the diffusion problem $\kappa_{x_i x_i} \Delta f(x_i, t) = \delta f(x_i, t) / \delta t$ is well known as a Gaussian function with the width of the distribution described via the diffusion coefficient $\kappa_{x_i x_i}$. Building the second moment of the deviation in x_i provides an analytical solution, $\langle \Delta x_i^2 \rangle = 2t \kappa_{x_i x_i}$. The left-hand side of this equation can be calculated in simulations of particles that are emitted from a point source, which is placed in a field

composed of a homogeneous component $\vec{B} = B \vec{e}_z$ and a turbulent one $b = |\vec{b}|$. Here, we use a Kolmogorov-type spectrum, i.e., isotropic and without intermittency:

$$G(k) \propto \begin{cases} 0 & \text{if } k < k_{\min}, \\ \left(\frac{k}{k_{\min}}\right)^{-\alpha} & \text{if } k_{\min} \leq k \leq k_{\max} \\ 0 & \text{if } k_{\max} < k, \end{cases} \quad (1)$$

with $k_{\min} = 2\pi/l_{\max}$, $k_{\max} = 2\pi/l_{\min}$, and $\alpha = 5/3$. The correlation length in the limit $l_{\min}/l_{\max} \ll 1$ yields $l_c = l_{\max}/5$ [23].

For discrete step sizes $s_{\text{step}} = v \Delta t$, the diffusion coefficient can be calculated as

$$\kappa_{ii}(t) = \sum_{n=0}^{t/(\Delta t)} \Delta t \langle v_i(n\Delta t) v_i(0) \rangle = \sum_{n=0}^{t/(\Delta t)} \langle v_i(n\Delta t) \Delta x_i(0) \rangle. \quad (2)$$

i indicates the three spatial directions. Here, we only consider parallel diffusion $\kappa \equiv \kappa_{ii} = \kappa_{\parallel}$. The perpendicular component will be discussed elsewhere. Further, $t = n \Delta t$ is the time after n time steps. We propagate particles on a grid with $N_{\text{grid}} = 1024$, $s = 0.17$ pc, $l_{\min} = 1.7$ pc and $l_{\max} = 82.45$ pc. With the large grid and correspondingly broad spectrum, particles always find waves for interactions [24]. The comparatively large $l_{\min} = 10s$ [24] is chosen in order to reduce interpolation errors. In [24] it is shown that due to the interpolation of the turbulent magnetic field the magnetic wavevector spectrum ($a > 5/3$) can deviate from a Kolmogorov-type spectrum and becomes relevant for the lowest rigidities. We therefore chose $\rho = 0.3$ as an absolute lower boundary in the fits (see supplemental material) to exclude the numerical effects.

For Gaussian particle distributions, the running diffusion coefficient $\kappa(t)$ is expected to converge in time to a constant value $\kappa(t) \rightarrow \kappa$. Simulation are stopped once converged, and the final value of the diffusion coefficient is taken as the steady-state one. We repeat these simulations for different reduced rigidities and fit a power law $\kappa \propto \rho^\gamma$ to the RSR range, where particles experience true diffusion: $l_{\min}/(\pi l_c(b/B)) < \rho < l_{\max}/(2\pi l_c)$. We test this for a broad range of turbulence levels $0.05 < b/B < 2$. The resulting spectral index as a function of b/B is shown in Fig. 2. The QLT limit of $\gamma = 1/3$ is not yet reached at the 5% turbulence level, but is expected to at even lower b/B . At $b/B = 1$, the upper limit for diffusion is reached, consistent with Bohm diffusion $\kappa \propto \rho^1$.

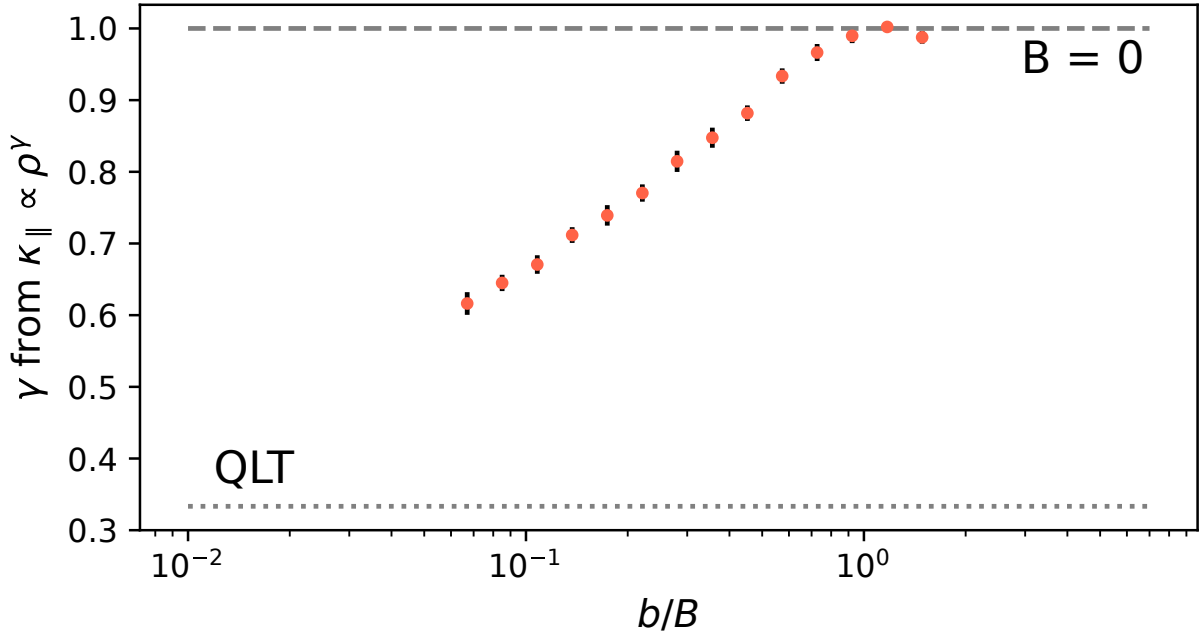


FIG. 2. Spectral index of the diffusion coefficient in the RSR with statistical errors. The simulated diffusion coefficients are fitted linearly in the log-log representation for each ratio of b/B as shown in the supplement, with the slopes shown in this plot. The errors increase towards low ratios of b/B , due to the decreasing range of the RSR as consequently fewer data points available for the fits. The simulation parameters are: $l_{\min} = 1.7$ pc, $l_{\max} = 82.45$ pc, $l_c = 17.8$ pc, $s = 0.17$ pc, $N_{\text{grid}} = 1024$. Due to the decreasing range of the RSR for smaller b/B , the fits are performed with fewer data points, leading to an increasing error.

DISCUSSION AND OUTLOOK

The two key findings of this work are

1. The energy range for diffusive propagation is highly constrained. In the ideal situation, where a simulation covers the entire wavevector spectrum with a physical k_{\min} and k_{\max} , the five regimes we present are physical and need to be considered in cosmic-ray propagation. It should be noted that our interpretation of the regions below and above the resonant scattering regime can change if we go from having sharp cutoffs in the wavevector spectrum [Eq. (1)]. In particular, in the mirror regime, more waves for scattering will be available and the effect in the MR will be reduced and only become more prominent toward the boundary of the NRSR. Conclusions about the

RSR, NRSR and QBR stay the same. In particular, our results presented on the diffusion coefficient are unaffected.

2. By selecting an appropriate range for the fits to the energy dependence of the particles, we quantitatively show for the first time that QLT is *not* valid at turbulence levels higher than 5% for Kolmogorov turbulence. Around $b/B \sim 1$, the Bohm diffusion limit $\kappa \propto \rho^1$ is reached. Qualitatively, the steeper energy dependence of the diffusion coefficient at larger b/B occurs because higher energy particles “see” the larger-amplitude turbulence first and start transitioning to the Bohm regime before lower-energy particles do. A more quantitative explanation of this effect is beyond the scope of this paper and will be addressed in forthcoming work.

These results can be put into an astrophysical context, specifically diffuse gamma-ray emission from the Milky Way. A radial gradient exists in the proton spectral index observed in the Galaxy [25] — the cosmic-ray spectrum in the central molecular zone, i.e., the inner 200 pc, is very flat, with $dN/dE \propto E^{-2.3}$. At a radius of 0.2 – 1.5 kpc from the Galactic Center (GC), the spectrum becomes extremely steep, $E^{-3.1}$, then reflattening to about $E^{-2.6} - E^{-2.7}$ up to 8 kpc. In the outskirts of the Galaxy at > 8 kpc, the spectrum becomes steeper again with $E^{-2.8} - E^{-2.9}$; compare Ref. [26].

Cosmic-ray self-confinement via the streaming instability [17] has an influence on the spectrum. However, this requires cosmic-ray energies below which the cosmic ray flux, which excites the instability, is large enough to overcome damping by the thermal background. It has long been recognized that above this critical energy, there must be a transition to confinement by turbulence from another source. Estimates for this critical energy are in the 100 – 300 GV range, depending on the damping mechanism ([14, 27, 28]). This could produce a spectral break as observed in cosmic-ray data [28, 29]. It is unclear, however, if the instability can be maintained up to energies as high as 100 GV [30]. It is also beyond the scope of this work to tie this to a trend with galactocentric radius and we simply point here that such an influence needs to be taken into account for a full simulation of Galactic propagation.

Galactocentric effects that could cause the steepening in the spectrum can be divided into data reduction problems and transport-related phenomena. We provide a list and argue that our present findings support argument number 5:

1. Unresolved point sources can play an important role. While Ref. [31] argues that this contribution should be negligible, its role is not fully understood [32].
2. A limited understanding of the gas distribution, and with it a possible systematic error in the data cannot be excluded. This is particularly true for the central volume with $r < 1$ kpc [25], which could have steeper cosmic ray spectra. However, data at TeV energies exist indicating that the local spectrum is quite flat [33].
3. A Galactic wind keeps the spectral behavior of observed cosmic rays constant at the level of injection. This would explain the observed flat component in the central molecular zone assuming the dominance of the wind in the Galactic Center region [31, 34].
4. A geometric effect of different orientations of the total magnetic field along the galactocentric radius [35] could contribute to the gradient.
5. Deviations from Kolmogorov-type diffusion in QLT have been discussed [35]. A radial dependence of the spectral index of the diffusion coefficient in the Galaxy has been proposed to explain the spectral softening toward the outer parts of the Galaxy [34], i.e., $\alpha = B + Ar$.

This last effect, which has commonly been employed as a phenomenological explanation [34, 35], can now be supported by fundamental arguments: The turbulence level increases toward the outer parts of the Galaxy [36–38]. With the increase of the diffusion spectral index toward higher turbulence levels, we expect the spectrum toward large galactocentric radii to become steeper. Our results indicate that the scenario of a diffusion-driven change in the spectral index needs to be taken into account when trying to explain the cosmic-ray gradient problem in the Galaxy. Future work on detailed simulations of Galactic transport, including the b/B dependence as derived here, in comparison with state-of-the-art observations will help to discriminate the different scenarios.

We would like to thank Paolo Desiati, Andrej Dundovic, Horst Fichtner, Rainer Grauer, Gwenael Giacinti, Isabelle Grenier, Reinhard Schlickeiser, Andreas Shalchi and Anvar Shukurov for highly valuable discussions. We acknowledge support from U.S. DOE grant DE-FG02-04ER-54742 (MJP) and NSF grant AST 1616037 (EGZ). Simulations were performed with CRPropa [39], supported by various analysis tools [40–43].

APPENDIX A: SCALING OF THE RESULTS WITH REDUCED RIGIDITY

Given the prediction of QLT, $\kappa_{\parallel} = cl_c(r_g/l_c)^\gamma(B/b)^2$ makes the problem rescalable for a different range of energies E , magnetic field properties b, B, l_c and the particle's electric charge q :

$$\kappa_{\parallel} = 9.494 \cdot 10^{27} \text{cm}^2/\text{s} \cdot 0.9251^{-\gamma+1/3} \cdot \left(\frac{b}{0.1 \mu\text{G}}\right)^{-2} \left(\frac{B}{\mu\text{G}}\right)^{2-\gamma} \left(\frac{E}{10 \text{PeV}}\right)^{-2} \left(\frac{l_c}{10 \text{pc}}\right)^{-2} \left(\frac{q}{e}\right)^{-2}. \quad (3)$$

The boundaries of the RSR derived within this study can be rescaled analogously as follows

$$E_{\min} = 2.945 \text{PeV} \left(\frac{b}{0.1 \mu\text{G}}\right)^{-1} \left(\frac{B}{\mu\text{G}}\right) \left(\frac{l_{\min}}{\text{pc}}\right) \left(\frac{q}{e}\right), \quad (4)$$

for the lower boundary E_{\min} of the RSR and

$$E_{\max} = 14.72 \text{PeV} \left(\frac{B}{\mu\text{G}}\right) \left(\frac{l_{\max}}{\text{pc}}\right) \left(\frac{q}{e}\right) \quad (5)$$

for the upper boundary E_{\max} . The diffusion process of particles is consequently not limited to a certain range of energies, but can be rescaled accordingly assuming that (a) the power-law behavior can be extended to the entire range of the turbulence spectrum, (l_{\min}, l_{\max}) and (b) assuming that the (b/B) -dependence is as expected in Eq. (3). We find evidence in our simulations that the $(b/B)^{-2}$ -dependence holds (Reichherzer et al., in prep). Therefore, scaling can be considered applicable in several astrophysical environments as demonstrated with two examples of cosmic ray propagation sites:

1. *Heliosphere*: Typical magnetic field parameters at 1 AU in the heliosphere are $b/B \approx 0.4 - 1$ [44], $B \sim 5 \text{nT}$ [45, 46] as well as $l_{\min} \sim 0.1 \text{AU}$ and $l_{\max} \sim 30 \text{AU}$ [47]. Here, the RSR for protons is within $1 - 3 \text{GeV} \lesssim E \lesssim 107 \text{TeV}$.
2. *Galaxy*: The magnetic waves of the turbulence range between the dissipation scale $l_{\min} \sim 1 \text{AU}$ to the maximum scale $l_{\max} \sim 150 \text{pc}$ in the halo and $l_{\max} \sim 20 \text{pc}$ in the disk [48]. Assuming $B \sim \mu\text{G}$ and $b \sim 0.1 \mu\text{G}$ constrains the RSR within $14 \text{GeV} \lesssim E_{\text{halo}} \lesssim 22 \text{PeV}$ and $14 \text{GeV} \lesssim E_{\text{disk}} \lesssim 3 \text{PeV}$ for protons.

These are only two examples, the equations can be rescaled for different astrophysical boundary conditions as shown above.

APPENDIX B: DESCRIPTION OF FITS TO THE RIGIDITY SPECTRA

In Figure 3 we show the simulation results of the diffusion coefficients calculated using 5000 particles in each simulation for 14 different ratios of b/B , where $B = 1 \mu\text{G}$ was kept constant. For each of these ratios up to 21 different energies are simulated. Further parameters are: The statistical errors of the diffusion coefficients are calculated by repeating each simulation 20 times with different realisations of the turbulent magnetic field. These are in total more than 5500 simulations. The averaged diffusion coefficients are shown as functions of the reduced rigidity in Fig. 3 together with their statistical uncertainties, which are, however, too small to be visible. We perform fits in the RSR to determine the energy scaling of the diffusion coefficients for different ratios of b/B . The turbulence interpolation effect becomes relevant at $\rho \lesssim 0.3$ and we therefore fit the data only above this value. The statistical uncertainties are determined by the number of data points taken into account in the fit. As the number of considered data points decreases for the four weakest fluctuation levels, the uncertainties also increases. The low uncertainties for large ratios of b/B in the fits do not necessitate the consideration of any further data points.

APPENDIX C: GENERAL STRUCTURE OF THE ENERGY DEPENDENCY OF THE DIFFUSION COEFFICIENTS

We present simulated diffusion coefficients as functions of reduced rigidity in Fig. 4. The different fluctuation ranges demonstrate the dependence of the upper boundary of the NRSR on l_{\min} , indicated by the vertical dashed-dotted colored lines. The upper boundary of the RSR is independent of l_{\min} and l_{\max} as long as l_c is constant. Due to the small distances between l_{\min} and l_{\max} the approximation $l_c = l_{\max}/5$ becomes inaccurate, therefore the exact definition of the correlation length is used for these simulations [49]:

$$l_c = \frac{l_{\max}}{2} \frac{\alpha - 1}{\alpha} \frac{1 - (l_{\min}/l_{\max})^\alpha}{1 - (l_{\min}/l_{\max})^{\alpha-1}}. \quad (6)$$

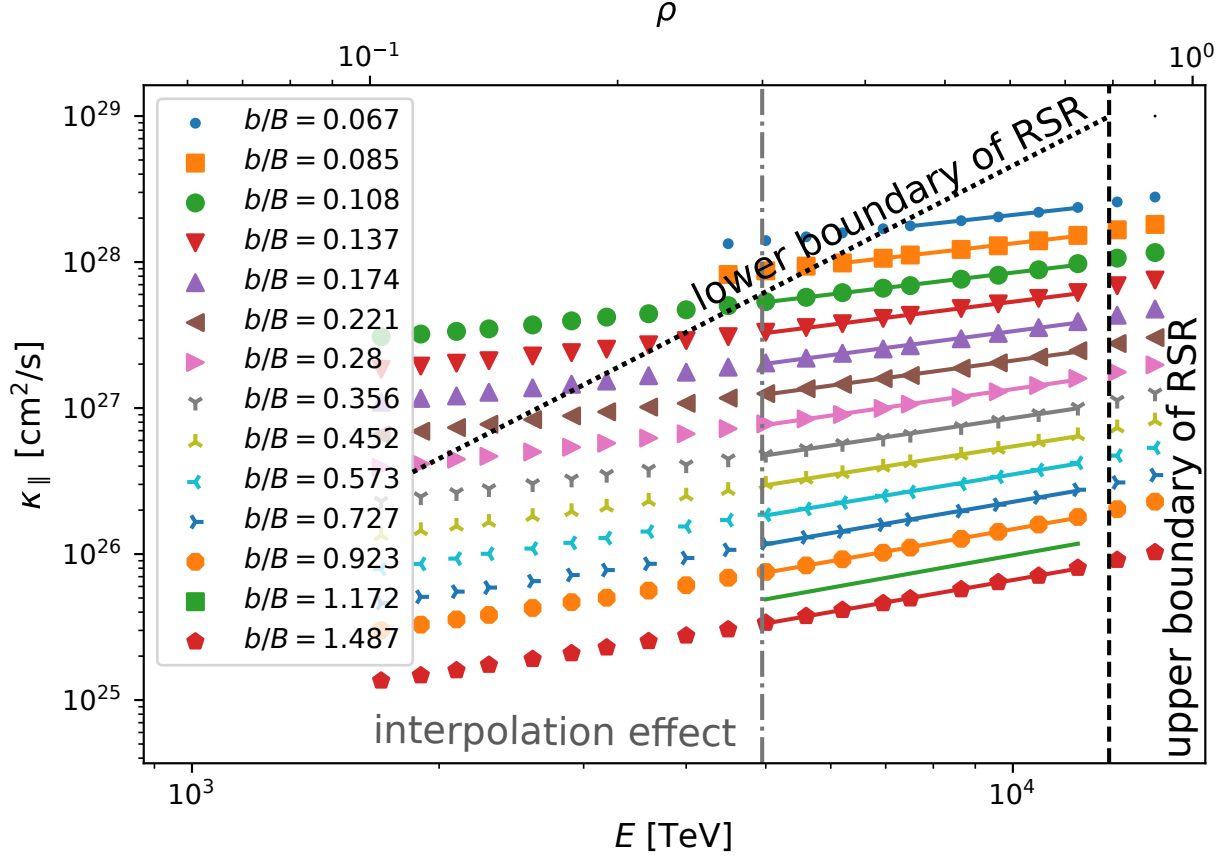


FIG. 3. Parallel diffusion coefficients as functions of ρ and E . Simulation results below the lower boundary of RSR $\rho \lesssim l_{\min}/(\pi(b/B)l_c)$, below the line indicating a noticeable effect of interpolation and above the upper boundary of RSR are ignored. Fits are performed to the remaining simulation data. The parameters are: $l_{\min} = 1.7$ pc, $l_{\max} = 82.45$ pc, $l_c = 17.8$ pc, $s = 0.17$ pc, $N_{\text{grid}} = 1024$. Each data point represent the mean of 20 diffusion coefficients, each simulated with the same parameters, but with a different turbulent field. Due to the decreasing range of the RSR for smaller b/B , the fits are performed with fewer data points, leading to an increasing error in the slopes of the fits.

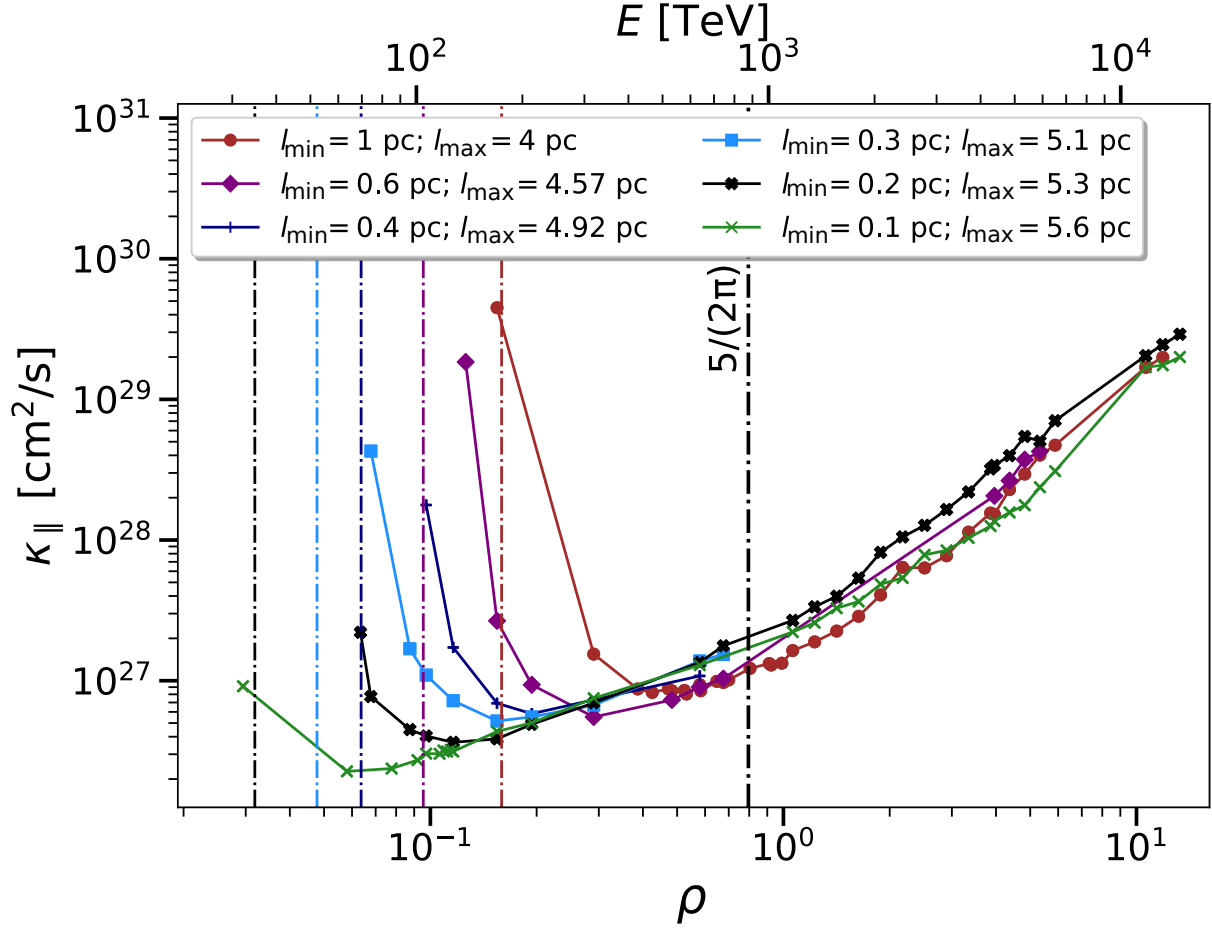


FIG. 4. Diffusion coefficients as functions of the reduced rigidity for different ranges of fluctuation scales l . The black dash-dotted line represents the upper boundary of the RSR, while the colored dash-dotted lines indicate the boundaries between NRSR and MR for a given set of scales. Simulated with a turbulent field $b = 0.1 \mu\text{G}$ together with a background field $B = 1 \mu\text{G}$.

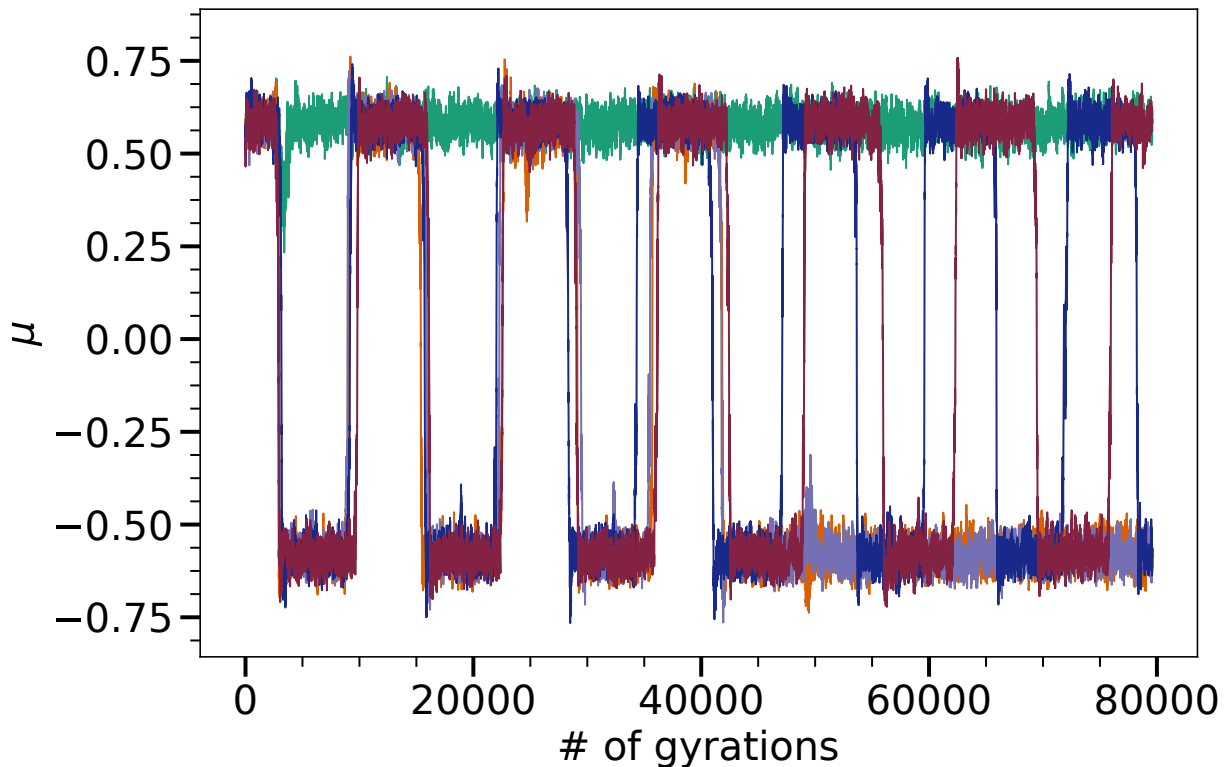


FIG. 5. The pitch angles $\mu = \cos \theta$ of five particles are shown as functions of the number of gyrations in the background field. The particles are injected with $\mu = 0.5$, $E = 100$ TeV, $b/B = 0.015$ and $B = 1 \mu\text{G}$.

APPENDIX D: MIRRORING

The strong occurrence of the mirroring effect for five exemplary particle trajectories for low energy particles is demonstrated in Fig. (5). Here, the pitch angle $\mu = \cos \theta$ of each particle is shown as a function of the travelled distance in number of gyrations. After traveling a certain distance along the background magnetic field, they turn around due to a magnetic bottle that is generated in the magnetic field.

-
- [1] A. W. Strong and I. V. Moskalenko, (1998).
 - [2] C. Evoli *et al.*, *J. Cosm. and Astr. Phys.* **10**, 018 (2008).
 - [3] R. Kissmann, *Astropart. Phys.* **55**, 37 (2014), arXiv:1401.4035 [astro-ph.HE].

- [4] V. S. Berezhinskii, S. V. Bulanov, V. A. Dogiel, and V. S. Ptuskin, *Amsterdam: North-Holland, 1990, edited by Ginzburg, V.L.* (1990).
- [5] A. Kolmogorov, *Akademiia Nauk SSSR Doklady* **30**, 301 (1941).
- [6] J. R. Jokipii, *Astroph. J.* **146**, 480 (1966).
- [45] J. Giacalone and J. R. Jokipii, *The Astrophysical Journal* **520**, 204 (1999).
- [8] F. Casse, M. Lemoine, and G. Pelletier, *Phys. Rev.* **D65**, 023002 (2002), arXiv:astro-ph/0109223 [astro-ph].
- [9] D. D. Marco, P. Blasi, and T. Stanev, *Journal of Cosmology and Astroparticle Physics* **2007**, 027 (2007).
- [10] J. Minnie, J. W. Bieber, W. H. Matthaeus, and R. A. Burger, *The Astrophysical Journal* **663**, 1049 (2007).
- [11] Lange, S., Spanier, F., Battarbee, M., Vainio, R., and Laitinen, T., *A&A* **553**, A129 (2013).
- [12] A. P. Snodin, A. Shukurov, G. R. Sarson, P. J. Bushby, and L. F. S. Rodrigues, *Mon. Not. Roy. Astron. Soc.* **457**, 3975 (2016), arXiv:1509.03766 [astro-ph.HE].
- [13] G. Giacinti, M. Kachelriess, and D. V. Semikoz, *JCAP* **1807**, 051 (2018), arXiv:1710.08205 [astro-ph.HE].
- [14] C. J. Cesarsky and R. M. Kulsrud, *Astroph. J.* **185**, 153 (1973).
- [15] G. M. Felice and R. M. Kulsrud, *Astroph. J.* **553**, 198 (2001).
- [16] A. Seta, A. Shukurov, T. S. Wood, P. J. Bushby, and A. P. Snodin, *Mon. Not. Roy. Astron. Soc.* **473**, 4544 (2018), arXiv:1708.07499.
- [17] R. Kulsrud and W. P. Pearce, *Astroph. J.* **156**, 445 (1969).
- [18] N. Globus, D. Allard, and E. Parizot, *Astron. Astrophys.* **479**, 97 (2008), arXiv:0709.1541 [astro-ph].
- [19] G. Sigl, *Astroparticle Physics: Theory and Phenomenology*, Atlantis Studies in Astroparticle Physics and Cosmology (Atlantis Press, 2017).
- [20] J. W. Armstrong, B. J. Rickett, and S. R. Spangler, *Astroph. J.* **443**, 209 (1995).
- [21] A. Shalchi, ed., *Astrophysics and Space Science Library*, Astrophysics and Space Science Library, Vol. 362 (2009).
- [22] P. Subedi, W. Sonsrtee, P. Blasi, D. Ruffolo, W. H. Matthaeus, D. Montgomery, P. Chuychai, P. Dmitruk, M. Wan, T. N. Parashar, and R. Chhiber, *The Astrophysical Journal* **837**, 140 (2017).

- [23] D. Harari, S. Mollerach, and E. Roulet, *Phys. Rev. D* **89**, 123001 (2014).
- [24] L. Schlegel, A. Frie, B. Eichmann, P. Reichherzer, and J. Becker Tjus, arXiv:1907.09934 (2019).
- [25] F. Acero, M. Ackermann, M. Ajello, A. Albert, L. Baldini, J. Ballet, G. Barbiellini, D. Bastieri, R. Bellazzini, and E. Bissaldi, *Astroph. J. Suppl. Series* **223**, 26 (2016), arXiv:1602.07246 [astro-ph.HE].
- [26] R. Yang, F. Aharonian, and C. Evoli, *Phys. Rev. D* **93**, 123007 (2016), arXiv:1602.04710 [astro-ph.HE].
- [27] A. J. Farmer and P. Goldreich, *Astroph. J.* **604**, 671 (2004), arXiv:astro-ph/0311400 [astro-ph].
- [28] *Physical Review Letters* **109**, 061101 (2012), 10.1103/PhysRevLett.109.061101, arXiv:1207.3706 [astro-ph.HE].
- [29] C. Evoli, R. Aloisio, and P. Blasi, *Phys. Rev. D* **99**, 103023 (2019), arXiv:1904.10220 [astro-ph.HE].
- [30] R. Schlickeiser, M. Caglar, and A. Lazarian, *Astroph. J.* **824**, 89 (2016).
- [31] M. Pothast, D. Gaggero, E. Storm, and C. Weniger, *J. Cosm. and Astr. Phys.* **2018**, 045 (2018), arXiv:1807.04554 [astro-ph.HE].
- [32] I. Grenier, (2019), private communication.
- [33] A. Abramowski *et al.*, *Nature* **531**, 476 (2016).
- [34] D. Gaggero, D. Grasso, A. Marinelli, M. Taoso, and A. Urbano, *Phys. Rev. Lett.* **119**, 031101 (2017), arXiv:1702.01124 [astro-ph.HE].
- [35] D. Gaggero, A. Urbano, M. Valli, and P. Ullio, *Phys. Rev. D* **91**, 083012 (2015), arXiv:1411.7623 [astro-ph.HE].
- [36] R. Jansson and G. R. Farrar, *The Astrophysical Journal* **757**, 14 (2012).
- [37] J. Kleimann, T. Schorlepp, L. Merten, and J. Becker Tjus, *Astroph. J.* **877**, 76 (2019), arXiv:1809.07528 [astro-ph.GA].
- [38] A. Shukurov, L. F. S. Rodrigues, P. J. Bushby, J. Hollins, and J. P. Rachen, *Astron. & Astroph.* **623**, A113 (2019), arXiv:1809.03595 [astro-ph.GA].
- [39] R. Alves Batista, A. Dundovic, M. Erdmann, K.-H. Kampert, D. Kuempel, G. Müller, G. Sigl, A. van Vliet, D. Walz, and T. Winchen, *J. Cosm. and Astr. Phys.* **5**, 038 (2016), 10.1088/1475-7516/2016/05/038.

- [40] S. van der Walt, C. S. Colbert, and G. Varoquaux, *Computing in Science & Engineering* **13** (2011), 10.1109/MCSE.2011.37.
- [41] J. D. Hunter, *Computing In Science & Engineering* **9** (2007), 10.1109/MCSE.2007.55.
- [42] T. Kluyver, B. Ragan-Kelley, F. Pérez, B. Granger, M. Bussonnier, J. Frederic, K. Kelley, J. Hamrick, J. Grout, S. Corlay, P. Ivanov, D. Avila, S. Abdalla, and C. Willing, in *Positioning and Power in Academic Publishing: Players, Agents and Agendas*, edited by F. Loizides and B. Schmidt (IOS Press, 2016) pp. 87 – 90.
- [43] W. McKinney, in *Proceedings of the 9th Python in Science Conference*, edited by S. van der Walt and J. Millman (2010) pp. 51 – 56.
- [44] R. Bruno and V. Carbone, *Living Reviews in Solar Physics* (2013) 10: 2. doi:10.12942/lrsp-2013-2.
- [45] J. Giacalone and J. R. Jokipii, *The Astrophysical Journal* **520**, 204 (1999).
- [46] L. Adhikari *et al.*, *The Astrophysical Journal* **841** (2013) no. doi:10.12942/lrsp-2013-2.
- [47] G. Zank, W. Matthaeus and C. Smith, *Journal of Geophysical Research*. **101** (1996). doi:10.1029/96JA01275.
- [48] M. Iacobelli *et al.*, *Astron. Astrophys.* **558**, A72 (2013) doi:10.1051/0004-6361/201322013 [arXiv:1308.2804 [astro-ph.GA]].
- [49] D. Harari, S. Mollerach and E. Roulet, *Phys. Rev. D* **89** (2014) no.12, 123001 doi:10.1103/PhysRevD.89.123001 [arXiv:1312.1366 [astro-ph.HE]].